As per UGC guidelines an electronic bar code is provided to secure your paper

International Journal for Modern Trends in Science and Technology
Volume 12, Issue 07, pages 232-246.
ISSN: 2455-3778 online
Available online at: http://www.ijmtst.com/vol12issue06.html
DOI: https://doi.org/10.5281/zenodo.21535191

Design and Control of a Solar PV and Wind Energy Based EV Charging Station with Active Harmonic Mitigation for Three-Phase Grid Applications

C. Jyothi Prakash | K. Venkatapathi | Dr. K. Siva Kumar

Department of Electrical & Electronics Engineering, Sri Venkatesa Perumal College of Engineering and Technology, Puttur, Andhra Pradesh, India.

To Cite this Article
C. Jyothi Prakash, K. Venkatapathi & Dr. K. Siva Kumar (2026). Design and Control of a Solar PV and Wind Energy Based EV Charging Station with Active Harmonic Mitigation for Three-Phase Grid Applications. International Journal for Modern Trends in Science and Technology, 12(07), 232-246. https://doi.org/10.5281/zenodo.21535191

Article Info
Received: 18 June 2026; Revised: 18 July 2026; Accepted: 23 July 2026.

KEYWORDS

Active harmonic mitigation, battery energy storage system (BESS), bidirectional DC–DC buck–boost converter, electric vehicle charging station, hybrid renewable energy system, maximum power point tracking (MPPT), permanent magnet synchronous generator (PMSG), power quality, shunt active power filter (SAPF).

ABSTRACT

This paper presents the design and control of a hybrid solar photovoltaic (PV) and wind energy based electric vehicle (EV) charging station with active harmonic mitigation for three-phase grid applications. The proposed system integrates a solar PV array, a permanent magnet synchronous generator (PMSG)-based wind energy conversion system, battery energy storage, and an EV charging station through a common DC-link to provide reliable and sustainable power. A DC–DC boost converter with maximum power point tracking (MPPT) is employed to maximize power extraction from the renewable energy sources, while a bidirectional DC–DC buck–boost converter regulates battery charging and discharging and maintains a stable DC-link voltage. A three-phase voltage source converter (VSC) connected through an LCL filter operates as a shunt active power filter using synchronous reference frame (SRF) control and hysteresis current control to compensate harmonic currents, provide reactive power compensation, and improve grid power quality. The coordinated control strategy enables effective power sharing among the renewable sources, battery storage, utility grid, and EV charging station under varying operating conditions. MATLAB/Simulink simulation results demonstrate improved renewable energy utilization, stable DC-link voltage regulation, efficient EV charging, reduced current harmonics, and enhanced overall system performance. The proposed hybrid renewable energy-based EV charging station offers an efficient, reliable, and environmentally sustainable solution for future smart grid and electric transportation applications.

1. INTRODUCTION

The rapid increases in global energy demand, depletion of conventional fossil fuel resources, and growing environmental concerns have accelerated the transition toward renewable energy-based power generation systems. Among various renewable energy technologies, solar photovoltaic (PV) and wind energy have emerged as the most promising clean energy sources because of their abundant availability, environmental sustainability, and declining installation costs [1]. Simultaneously, the transportation sector is experiencing a revolutionary transformation through the widespread adoption of electric vehicles (EVs), which offer significant reductions in greenhouse gas emissions and dependence on petroleum-based fuels [2]. The successful integration of renewable energy resources with EV charging infrastructure has therefore become an important research area for realizing sustainable smart grid applications. Electric vehicles are expected to dominate future transportation systems owing to stringent emission regulations, improved battery technologies, and government incentives promoting zero-emission transportation [3]. However, the increasing penetration of EV charging stations introduces considerable challenges to the existing electrical distribution network. High-power charging demands can result in voltage fluctuations, transformer overloading, feeder congestion, increased peak demand, and deterioration of overall power quality [4]. Moreover, the extensive utilization of power electronic converters in EV chargers introduces harmonic distortion, reactive power imbalance, and current waveform deformation, which adversely affect sensitive electrical equipment connected to the distribution network [5]. Consequently, advanced control strategies capable of maintaining grid stability while supporting efficient EV charging have become essential for future smart grid development. Renewable energy-powered EV charging stations represent an attractive solution to reduce dependence on utility grids while minimizing carbon emissions associated with electricity generation [6]. Solar PV generation has become one of the fastest-growing renewable technologies because of its modular structure, low maintenance requirements, and continuously decreasing installation costs [7]. Nevertheless, PV systems suffer from intermittent power generation caused by variations in solar irradiance and ambient temperature, resulting in fluctuating output power that limits reliable standalone operation [8]. Similarly, wind energy conversion systems provide clean electrical power but experience significant output variations due to continuously changing wind speeds [9]. These uncertainties necessitate the coordinated integration of multiple renewable sources together with suitable energy storage systems to ensure continuous and reliable operation. Hybrid renewable energy systems combining solar PV and wind generation provide complementary operating characteristics that significantly improve system reliability and energy availability compared with individual renewable sources [10]. During periods of low solar irradiation, wind energy may continue supplying electrical power, whereas solar generation can compensate during periods of reduced wind speed. Such complementary characteristics improve overall energy utilization, reduce renewable power curtailment, and enhance system operational flexibility [11]. Consequently, hybrid PV-wind generation has attracted considerable attention for supplying distributed loads, microgrids, and EV charging infrastructure with improved reliability and reduced dependence on conventional utility grids. Battery energy storage systems (BESS) further enhance the operational performance of hybrid renewable energy systems by balancing the mismatch between renewable generation and charging demand [12]. Energy storage devices absorb surplus renewable energy during periods of excess generation and discharge stored energy when renewable generation decreases or EV charging demand increases [13]. In addition, battery storage contributes to DC-link voltage stabilization, peak load shaving, renewable power smoothing, and improved system reliability [14]. Therefore, coordinated control of renewable generation, battery storage, and grid interaction is critical for maintaining uninterrupted EV charging services under varying environmental and loading conditions. Maximum power point tracking (MPPT) techniques play an essential role in maximizing energy extraction from renewable energy sources [15]. Since both solar irradiance and wind speed vary continuously throughout the day, the operating points of PV arrays and wind turbines change dynamically. Advanced MPPT algorithms enable renewable generators to operate at their respective maximum power points, thereby improving overall system efficiency and energy utilization [16]. DC–DC boost converters are widely employed to interface renewable generators with the common DC-link because of their simple structure, high conversion efficiency, and excellent voltage boosting capability [17]. These converters also facilitate independent control of renewable power extraction without disturbing the DC-link voltage. The bidirectional exchange of energy between battery storage and the common DC bus requires efficient bidirectional DC–DC converters capable of operating in both buck and boost modes [18]. During charging operation, excess renewable energy charges the battery through buck operation, whereas stored energy is supplied back to the DC-link through boost operation whenever renewable generation becomes insufficient. Appropriate converter control ensures stable battery charging, prevents excessive battery stress, and maintains continuous power availability for EV charging applications [19]. The bidirectional converter therefore serves as an essential component in improving the flexibility and operational stability of hybrid renewable energy systems. Power electronic converters are indispensable in renewable energy-based EV charging stations; however, their switching operations generate harmonic currents that degrade power quality and reduce overall system efficiency [20]. Harmonic distortion increases transformer losses, causes overheating of electrical equipment, interferes with communication systems, and shortens equipment lifetime. Moreover, nonlinear EV charging loads contribute additional harmonic currents and reactive power demand, further deteriorating the quality of power supplied by the utility grid [21]. Therefore, harmonic mitigation has become a major design consideration in grid-connected renewable energy systems. Among various harmonic compensation techniques, shunt active power filters (SAPFs) have demonstrated excellent performance because of their capability to compensate harmonic currents dynamically under varying load conditions [22]. Unlike passive filters, SAPFs effectively eliminate multiple harmonic orders, provide reactive power compensation, and improve current waveform quality without resonance problems [23]. The integration of SAPF functionality within the grid-connected voltage source converter significantly reduces system complexity and installation cost while simultaneously improving converter utilization. The synchronous reference frame (SRF) control technique has become one of the most widely adopted current control methods for three-phase active power filters because of its simple implementation, fast dynamic response, and excellent harmonic extraction capability [24]. By transforming three-phase currents into rotating dq reference coordinates, the SRF controller effectively separates fundamental active and reactive current components from harmonic components. Combined with hysteresis current control, the voltage source converter rapidly tracks the desired compensating current references, ensuring accurate harmonic cancellation and superior transient performance [25]. Furthermore, the incorporation of an LCL filter significantly suppresses switching-frequency harmonics injected into the utility grid while maintaining converter efficiency and reducing filter size [26]. Although numerous studies have investigated renewable energy integration, EV charging systems, battery storage, and active power filtering independently, comparatively fewer investigations have addressed the coordinated design of a hybrid solar PV and wind energy based EV charging station incorporating battery energy storage together with active harmonic mitigation under a unified control framework [27]. The coordinated interaction among renewable generators, battery storage, utility grid, and EV charging load requires efficient power management algorithms capable of ensuring stable DC-link regulation, continuous EV charging, renewable power maximization, harmonic compensation, and reactive power support simultaneously [28]. To address these challenges, this paper proposes a comprehensive hybrid renewable energy-based EV charging station integrating solar PV generation, a permanent magnet synchronous generator (PMSG)-based wind energy conversion system, battery energy storage, and a three-phase grid-connected voltage source converter with active harmonic mitigation capability. A DC–DC boost converter equipped with maximum power point tracking extracts maximum renewable power, whereas a bidirectional DC–DC buck–boost converter regulates battery charging and stabilizes the common DC-link voltage. The three-phase voltage source converter operates as a shunt active power filter using synchronous reference frame control and hysteresis current control to compensate harmonic currents, improve power factor, and provide reactive power compensation. The proposed coordinated control strategy enables efficient power sharing among renewable sources, battery storage, utility grid, and EV charging station under varying operating conditions while maintaining superior power quality. MATLAB/Simulink simulation results verify the effectiveness of the proposed system in achieving stable DC-link regulation, enhanced renewable energy utilization, efficient EV charging, significant harmonic reduction, and improved overall grid performance, demonstrating its suitability for future smart grid and sustainable transportation applications.

Main Contributions

The major contributions of this work are summarized as follows:

1. Developed a hybrid solar PV–wind EV charging station integrated with BESS for reliable and sustainable power supply.
2. Proposed an energy management strategy for coordinated power sharing among renewable sources, battery, grid, and EV charger.
3. Implemented a DC–DC boost converter with MPPT to maximize renewable energy extraction under varying conditions.
4. Designed a bidirectional DC–DC buck–boost converter for battery management and stable DC-link voltage regulation.
5. Employed a three-phase VSC as a Shunt Active Power Filter (SAPF) for harmonic mitigation and reactive power compensation.

Developed an SRF-based hysteresis current control for fast harmonic current compensation and improved grid power quality.

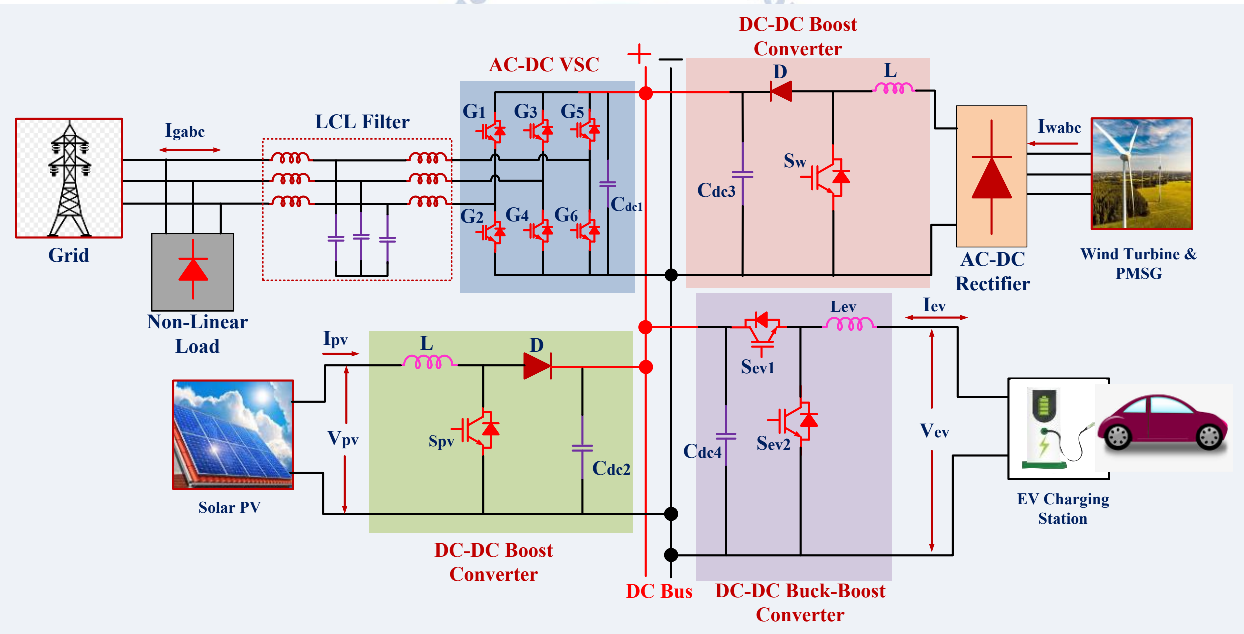

Fig. 1. Proposed Hybrid Renewable Energy-Based EV Charging Station

II. SYSTEM CONFIGURATION

The proposed hybrid EV charging station integrates a solar PV array, a PMSG-based wind energy conversion system, battery energy storage (BESS), and a three-phase utility grid through a common DC-link, as shown in Fig. 1. The solar PV and wind generation units are connected to the DC bus through dedicated DC–DC boost converters to maximize renewable energy extraction and regulate the DC-link voltage. A bidirectional DC–DC buck–boost converter interfaces the battery energy storage system, enabling controlled charging and discharging while maintaining a stable DC-link under varying operating conditions. The EV charging station is directly supplied from the common DC bus, ensuring efficient utilization of renewable energy and stored battery power. A three-phase Voltage Source Converter (VSC) connected through an LCL filter interfaces the system with the utility grid and operates as a Shunt Active Power Filter (SAPF). Using Synchronous Reference Frame (SRF) control together with hysteresis current control, the VSC compensates harmonic currents, provides reactive power support, improves the grid power factor, and maintains sinusoidal grid currents. The coordinated control strategy enables efficient power sharing among the renewable sources, battery storage, utility grid, and EV charging station, resulting in stable DC-link operation, reliable EV charging, enhanced renewable energy utilization, and improved overall system performance.

III. MODELING AND DESIGNING OF SOLAR PV CONFIGURATION

The solar photovoltaic (PV) system is one of the primary renewable energy sources employed in the proposed EV charging station. Owing to its clean, abundant, and sustainable nature, solar PV has become an attractive solution for grid-connected applications. In this work, the PV array is modeled using the widely adopted single-diode equivalent circuit, which accurately represents the nonlinear current-voltage (I–V) and power-voltage (P–V) characteristics of a PV cell under varying solar irradiance and temperature conditions. The PV cells are connected in series and parallel to form PV modules, which are further combined to construct the required PV array. As shown in Fig. 2, the PV array is connected to a DC–DC boost converter that regulates the output voltage and transfers the extracted power to the common DC-link.

The output current of the PV array based on the single-diode model is expressed as

$$I_{pv} = N_s I_s - N_p I_o\left(\exp\left(\frac{q(V_{pv}+R_s I_{pv})}{AkTN_s}\right)-1\right) - N_p\frac{V_{pv}+R_s I_{pv}}{N_s R_{sh}}$$
(1)

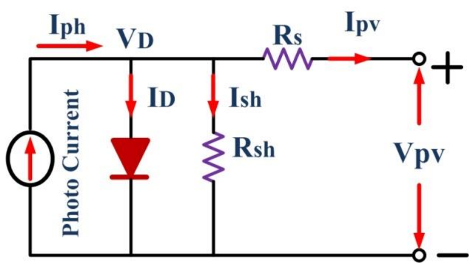

Fig 2: Equivalent circuit model of PV solar

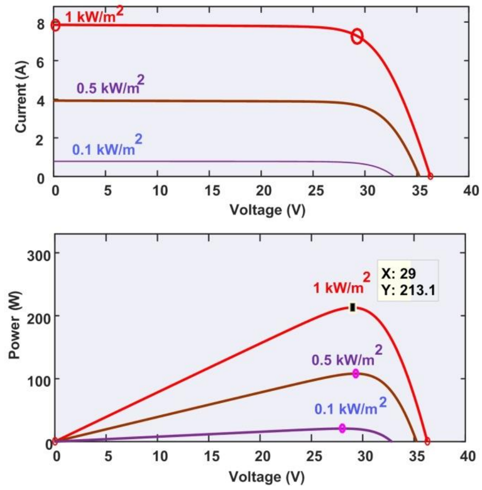

Fig 3: V–I and P–V characteristics of a single-diode PV solar cell

where Is is the light-generated current, Io is the diode reverse saturation current, R_s and R_{sh} are the series and shunt resistances, q is the electron charge, k is the Boltzmann constant, T is the cell temperature, and A is the diode ideality factor.

A. Solar PV Boost Converter

A DC–DC boost converter is employed to interface the PV array with the common DC-link. The converter increases the PV output voltage to the required DC-link voltage and enables maximum power extraction using the Perturb and Observe (P&O) Maximum Power Point Tracking (MPPT) algorithm. The P&O method continuously perturbs the operating voltage of the PV array and observes the corresponding change in output power. Based on the variation in power, the converter duty cycle is adjusted until the operating point reaches the maximum power point (MPP). This method provides a simple and effective solution for maximizing PV energy under changing irradiance conditions.

The steady-state voltage and current relationships of the boost converter are given by

The steady-state equations of the boost converter are:

- Boost converter output voltage:

$$V_o = \frac{V_{pv}}{1-D} \quad (2)$$

- Boost converter input current:

$$I_{pv} = \frac{I_o}{1-D} \quad (3)$$

Where: V_{pv} and I_{pv} is the PV voltage and current, V_o is the DC link voltage, Io is the output current, and D is the duty cycle. The MPPT algorithm continuously updates D to regulate V_{pv} around the MPP.

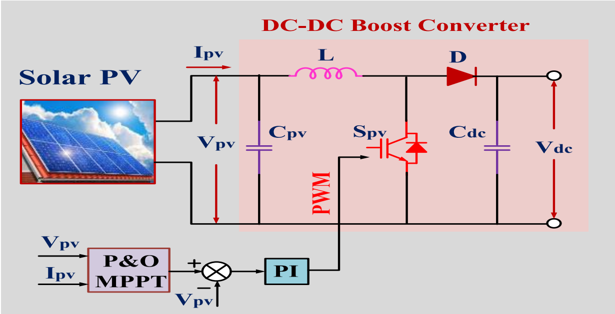

Fig 4: Solar PV P&O MPPT DC-DC boost converter

IV. MODELING AND DESIGNING OF LITHIUM-ION EV BATTERY

A. Electrochemical Fundamentals

Lithium-ion (Li-ion) batteries operate on the principle of reversible intercalation and de-intercalation of lithium ions between the graphite anode and a metal oxide cathode. The overall reaction of a Li-ion cell during charge–discharge is expressed as:

$$Li_xC + Li_{1-x}M_yO_z \Leftrightarrow C + L_iM_yO_z \quad (4)$$

Where:

- Li_xC represents the lithiated graphite anode,
- $Li_{1-x}M_yO_z$ represents the partially lithiated cathode (metal oxide such as $L_iC_0O_2, L_iF_ePO_4, LiMn_2O_4$),
- M is the transition metal,
- x denotes the degree of intercalation.
- At the anode (during discharge):
  $$Li_xC \longrightarrow C + xLi^+ + xe^- \quad (5)$$
- At the anode (during discharge):
  $$Li_{1-x}M_yO_z + xLi^+ \longrightarrow L_iM_yO_z \quad (6)$$

This reaction is reversible; enabling repeated charging and discharging cycles.

Electrical Modeling

Lithium-ion batteries are commonly represented using an Equivalent Circuit Model (ECM), which simplifies the underlying electrochemical processes while accurately capturing the electrical behavior. In this model, the terminal voltage of the cell is expressed as:

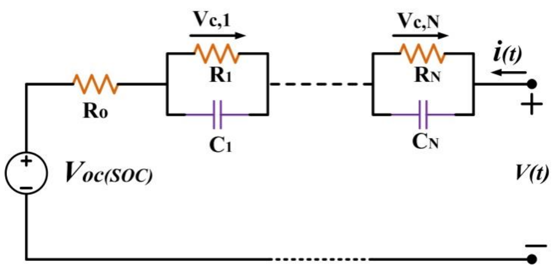

Fig 5: Equivalent circuit diagram of lithium ion EV battery

$$V(t) = V_{oc}(Soc) - I(t)R_s - V_{Rc}(t) \quad (7)$$

The battery terminal voltage $V(t)$ is influenced by the open-circuit voltage $V_{oc}(Soc)$, internal resistance Rs, and polarization voltage $V_{Rc}(t)$. This model effectively balances accuracy and simplicity, making it ideal for grid integration, renewable energy storage, and EV charging.

State of charge (SOC) measures the available charge relative to a battery's nominal capacity and changes over time based on the Coulomb counting principle.

$$SOC(t) = SOC(0) - \frac{1}{Q_{nom}} \int_0^t I(\tau)\, d\tau \quad (8)$$

Where $SOC(0)$ is the initial SOC, Q_{nom} is the nominal battery capacity in ampere-hours (Ah), and $I(\tau)$ is the instantaneous current (positive during discharge and negative during charge). Accurate modeling of both the ECM and SOC dynamics ensures reliable performance prediction, efficient energy management, and extended lifetime of lithium-ion batteries in modern power systems.

B. EV Charging System

The proposed electric vehicle (EV) charging system employs a bidirectional DC–DC buck–boost converter to facilitate power exchange between the common DC-link and the EV battery. The converter operates in Grid-to-Vehicle (G2V) mode during battery charging by stepping down the DC-link voltage to the required battery charging voltage. During Vehicle-to-Grid (V2G) operation, the converter operates in boost mode, allowing the stored battery energy to be transferred back to the DC-link and utility grid. This bidirectional power flow enhances system flexibility, supports renewable energy utilization, and improves overall energy management.

The dynamic behavior of the bidirectional DC–DC converter is represented using the state variables, namely the converter inductor current iL and the EV battery voltage Vev.

The state-space model is expressed as

$$\dot{x} = Ax + Bu \quad (9)$$

Where

$$x = \begin{bmatrix} i_L \\ V_{ev} \end{bmatrix} \quad (10)$$

$$A = \begin{bmatrix} 0 & -\frac{1-D}{L} \\ \frac{1-D}{C} & -\frac{1}{RC} \end{bmatrix} \quad (11)$$

$$B = \begin{bmatrix} \frac{1}{L} \\ 0 \end{bmatrix} \quad (12)$$

where L is the converter inductance, C is the output capacitance, R is the equivalent battery load resistance, and D is the converter duty cycle.

The output equation is given by

$$y = Cx \quad (13)$$

Where

$$C = [0 \quad 1] \quad (14)$$

The charging power delivered to the EV battery is expressed as

$$P_{EV} = V_{EV} I_{EV} \quad (15)$$

where V_{EV} and I_{EV} denote the battery voltage and charging current, respectively. The bidirectional converter ensures controlled power transfer between the DC-link and the EV battery, maintaining stable charging and discharging operation while supporting reliable integration of renewable energy sources in the proposed EV charging station.

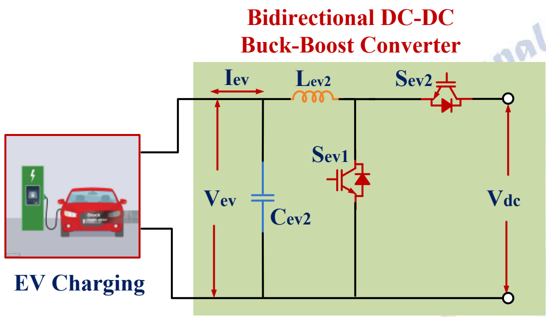

Fig 6: bidirectional dc-dc converter for EV.

The bidirectional DC–DC converter is regulated using a Proportional–Integral (PI) controller to achieve accurate battery current control and maintain stable DC-link operation. The controller generates the converter duty cycle by minimizing the error between the reference charging current and the measured battery current. The current error is defined as

$$e(t) = I_{ev}^{*} - I_{ev} \quad (16)$$

where I_{ev}^{*} is the reference charging current and I_{ev} is the measured charging current.

The control signal generated by the PI controller is expressed as

$$u(t) = K_p e(t) + K_i \int e(t)\, dt \quad (17)$$

where K_p and K_i denote the proportional and integral gains, respectively.

The controller output is used to determine the converter duty cycle,

$$D = u(t) \quad (18)$$

subject to the operating constraint

$$0 \leq D \leq 1 \quad (19)$$

to ensure safe and stable converter operation.

The charging power delivered to the EV battery is given by

The PI controller ensures smooth charging and discharging of the EV battery, maintains the DC-link voltage within the desired range, and enables reliable bidirectional power transfer between the battery, renewable energy sources, and the utility grid as shown in Fig.7. Its simple implementation and robust performance make it suitable for renewable energy-based EV charging applications.

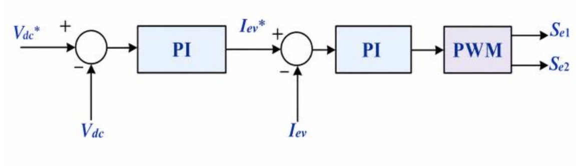

Fig. 7. Cascaded PI control structure for the bidirectional EV charging converter.

V. MODELING AND DESIGN OF PMSG-BASED WIND ENERGY CONVERSION SYSTEM

The proposed wind energy conversion system consists of a wind turbine, a Permanent Magnet Synchronous Generator (PMSG), a three-phase uncontrolled AC–DC rectifier, a DC–DC boost converter, and a Perturb and Observe (P&O) Maximum Power Point Tracking (MPPT) controller, as illustrated in Fig. 8. The wind turbine converts the kinetic energy of the wind into mechanical energy, which drives the PMSG to generate three-phase AC electrical power. The generated AC power is converted into DC through an uncontrolled diode bridge rectifier. Subsequently, a DC–DC boost converter regulates the rectified voltage and transfers the generated power to the common DC-link. The MPPT algorithm continuously adjusts the converter duty cycle to maximize the power extracted from the wind turbine under varying wind speed conditions.

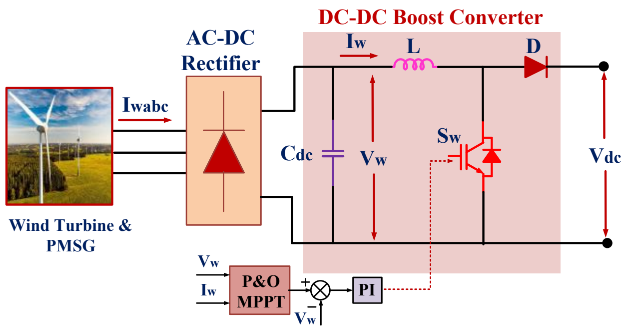

Fig. 8. Configuration of the PMSG-based wind energy conversion system.

The mechanical power extracted from the wind turbine is given by

$$P_m = \frac{1}{2}\rho A C_p(\lambda,\beta)V_w^3 \quad (20)$$

where ϱ is the air density (kg/m3), A is the swept area of the turbine blades (m2), Cp is the power coefficient, Vw is the wind speed (m/s), λ is the tip-speed ratio, and β is the blade pitch angle.

The tip-speed ratio is defined as

$$\lambda = \frac{R\,\omega_m}{V_w} \quad (21)$$

where R is the blade radius and ω_m is the rotor mechanical speed.

The mechanical torque developed by the wind turbine is

$$T_m = \frac{P_m}{\omega_m} \quad (22)$$

A. Mathematical Model of PMSG

The PMSG is modeled in the synchronously rotating dq-reference frame. The stator voltage equations are expressed as

$$= R_s i_d + L_d\frac{di_d}{dt} - \omega_e L_q i_q \quad (23)$$

$$V_q = R_s i_q + L_q\frac{di_q}{dt} + \omega_e L_q i_d + \omega_e\lambda_f \quad (24)$$

where

- Vd,Vq : dq-axis stator voltages (V)
- id,iq : dqdqdq-axis stator currents (A)
- Rs : stator resistance (Ω)
- Ld,Lq : dq-axis inductances (H)
- λ_f : permanent magnet flux linkage (Wb)
- ω_e : electrical angular speed (rad/s)

The electromagnetic torque is

$$T_e = \frac{3P}{4}\left[\lambda_f i_q + (L_d - L_q) i_d i_q\right] \quad (25)$$

For a surface-mounted PMSG,

$$L_d = L_q = L_s \quad (26)$$

Hence,

$$T_e = \frac{3P}{4}\lambda_f i_q \quad (27)$$

The rotor mechanical equation is

$$J\frac{d\omega m}{dt} = T_m - T_e - B_{\omega_m} \quad (28)$$

where

J is the rotor inertia and B is the viscous friction coefficient.

C. AC–DC Rectifier

The three-phase output voltage generated by the PMSG is converted into DC using an uncontrolled diode bridge rectifier. The average DC output voltage of the rectifier is

$$V_w = \frac{3\sqrt{2}}{\pi}V_{LL} \quad (29)$$

Where

VLL is the line-to-line RMS voltage of the PMSG.

D. DC–DC Boost Converter

The rectified DC voltage is regulated through a boost converter before being connected to the common DC-link.

The state variables are selected as

$$x = \begin{bmatrix} i_L \\ V_{dc} \end{bmatrix} \quad (30)$$

The converter dynamics are

$$\dot{x} = Ax + Bu \quad (31)$$

Where

$$A = \begin{bmatrix} 0 & -\frac{1-D}{L} \\ \frac{1-D}{C} & -\frac{1}{RC} \end{bmatrix} \quad (32)$$

$$B = \begin{bmatrix} \frac{1}{L} \\ 0 \end{bmatrix} \quad (33)$$

VI. PERTURB AND OBSERVE (P&O) MPPT ALGORITHM

The Perturb and Observe (P&O) Maximum Power Point Tracking (MPPT) algorithm is employed to maximize the power extracted from both the solar PV array and the PMSG-based wind energy conversion system. The algorithm continuously measures the output voltage and current of the renewable source to calculate the instantaneous output power. Based on the variation in power and voltage between two consecutive sampling instants, the operating point is adjusted toward the maximum power point (MPP) by updating the duty cycle of the corresponding DC–DC boost converter. Owing to its simple implementation and low computational complexity, the P&O algorithm is suitable for real-time renewable energy applications.

The instantaneous output power of the renewable source is given by

$$P(k) = V(k)I(k) \quad (34)$$

where V(k) and I(k) represent the measured voltage and current of the solar PV array or the rectified PMSG output at the kth sampling instant.

The change in output power is

$$\Delta P = P(k) - P(k-1) \quad (35)$$

and the change in voltage is

$$\Delta V = V(k) - V(k-1) \quad (36)$$

The reference voltage is updated according to the following decision rules:

If

$$\Delta P > 0\,,\, \Delta V > 0$$

$$V_{ref}(k) = V_{ref}(k-1) + \Delta V \quad (37)$$

If

$\Delta P > 0,\ \Delta V < 0$

$$V_{ref}(k) = V_{ref}(k-1) - \Delta V \quad (38)$$

If

$\Delta P < 0,\ \Delta V > 0$

$$V_{ref}(k) = V_{ref}(k-1) - \Delta V \quad (39)$$

If

$\Delta P < 0,\ \Delta V < 0$

$$V_{ref}(k) = V_{ref}(k-1) + \Delta V \quad (40)$$

The updated reference voltage is used to generate the duty cycle of the DC–DC boost converter according to

where V denotes the renewable source voltage (PV voltage or rectified PMSG voltage), Vdc is the boost converter output voltage, and D is the converter duty cycle.

For the solar PV system, the P&O algorithm continuously tracks the maximum power point under varying solar irradiance and temperature conditions. Similarly, for the PMSG-based wind energy conversion system, the algorithm regulates the boost converter duty cycle based on the rectified generator voltage and current, enabling maximum power extraction under varying wind speed conditions. Consequently, the proposed MPPT strategy improves renewable energy utilization, stabilizes the common DC-link voltage, and enhances the overall efficiency of the hybrid renewable energy-based EV charging station as shown in Fig.9.

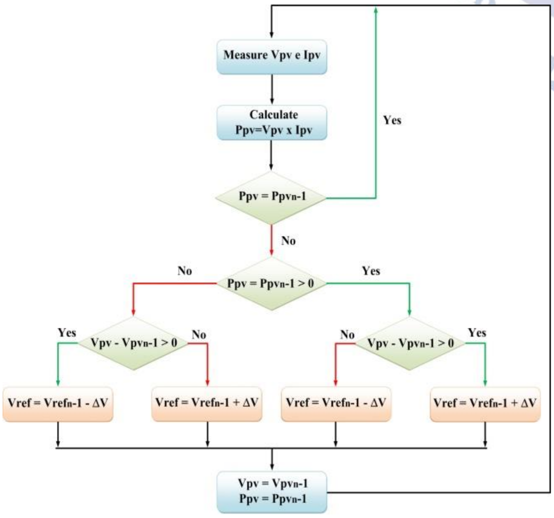

Fig 9: Flowchart of the P&O algorithm, implemented in the controller model.

VII. OPERATION OF THE GRID-CONNECTED AC–DC BIDIRECTIONAL CONVERTER

The proposed grid-connected AC–DC bidirectional converter, shown in Fig. 10, serves as the interface between the common DC-link and the three-phase utility grid. The converter consists of a three-phase Voltage Source Converter (VSC), an LCL filter, and a DC-link capacitor. The LCL filter effectively suppresses high-frequency switching harmonics generated by the converter, while the DC-link capacitor maintains a constant DC voltage to ensure stable operation of the renewable energy sources and EV charging station.

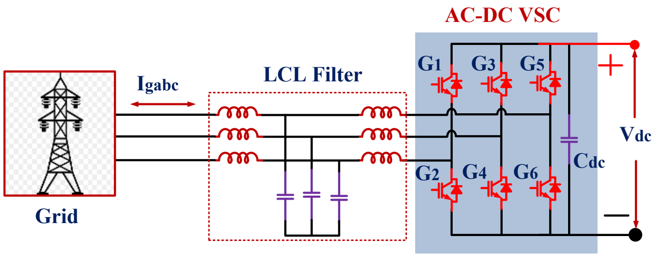

Fig. 10. Grid-connected bidirectional AC–DC voltage source converter (VSC)

The converter operates bidirectional to facilitate power exchange between the DC-link and the utility grid according to the available renewable power and EV charging demand. During periods of excess solar PV and wind power generation, the converter transfers surplus energy from the DC-link to the utility grid. Conversely, when renewable generation is insufficient to meet the charging demand, the converter imports power from the utility grid to maintain uninterrupted EV charging and a regulated DC-link voltage.

The dynamic behavior of the AC-side converter is described by

$$L_f \frac{di_g}{dt} = V_{inv} - V_g - R_f i_g \quad (41)$$

where L_f and R_f denote the filter inductance and resistance, respectively, V_{inv} is the converter output voltage, Vg is the grid voltage, and i_g is the grid current.

The DC-link capacitor dynamics are expressed as

$$C_{dc} \frac{dV_{dc}}{dt} = I_{dc} - I_{inv} \quad (42)$$

where C_{dc} is the DC-link capacitance, V_{dc} is the DC-link voltage, I_{dc} is the current supplied from the renewable energy sources, and I_{inv} is the converter input current.

The instantaneous active and reactive powers exchanged between the converter and the utility grid are given by

$$P = \frac{3}{2}(V_d i_d + V_q i_q) \quad (43)$$

$$Q = \frac{3}{2}(V_q i_d - V_d i_q) \quad (44)$$

where V_d and V_q are the grid voltage components, while i_d and i_q are the converter current components in the synchronous reference frame. The active power component regulates the DC-link voltage and controls the bidirectional power flow, whereas the reactive power component is controlled to achieve near-unity power factor.

In addition to bidirectional power transfer, the converter functions as a Shunt Active Power Filter (SAPF) by injecting compensating currents into the utility grid. This compensates harmonic currents generated by nonlinear loads and power electronic converters, thereby reducing current distortion and improving grid power quality. Consequently, the proposed AC–DC bidirectional converter ensures stable DC-link voltage regulation, efficient power transfer, harmonic current mitigation, reactive power compensation, and reliable integration of renewable energy sources with the utility grid.

VIII. SYNCHRONOUS REFERENCE FRAME (SRF)-BASED CONTROL OF GRID-CONNECTED AC–DC BIDIRECTIONAL CONVERTER

The grid-connected three-phase Voltage Source Converter (VSC) operates as a Shunt Active Power Filter (SAPF) to compensate harmonic currents, provide reactive power compensation, and regulate the common DC-link voltage. The converter is connected to the utility grid through an LCL filter, which suppresses high-frequency switching harmonics and improves current quality. The proposed control strategy employs the Synchronous Reference Frame (SRF) theory together with a Hysteresis Current Controller (HCC) to achieve accurate reference current generation and fast dynamic response under varying renewable generation and nonlinear load conditions as shown in Fig.11. The three-phase load currents are measured and transformed into the synchronous rotating dq-reference frame using the Clarke and Park transformations. The Clarke transformation converts the three-phase currents into the stationary $\alpha\beta$ reference frame as

$$\begin{bmatrix} i_\alpha \\ i_\beta \end{bmatrix} = \frac{2}{3}\begin{bmatrix} 1 & -\frac{1}{2} & -\frac{1}{2} \\ 0 & \frac{\sqrt{3}}{2} & -\frac{\sqrt{3}}{2} \end{bmatrix}\begin{bmatrix} i_a \\ i_b \\ i_c \end{bmatrix} \quad (45)$$

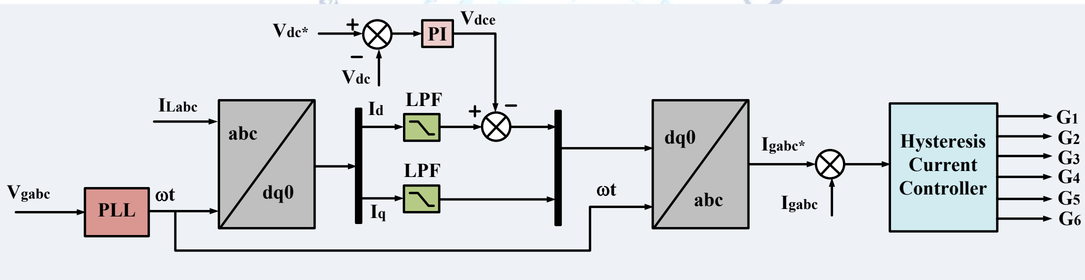

Fig. 11. SRF control of the bidirectional AC–DC converter.

The Park transformation converts the stationary frame into the synchronously rotating frame using the grid angle obtained from the Phase-Locked Loop (PLL),

$$\begin{bmatrix} i_d \\ i_q \end{bmatrix} = \begin{bmatrix} \cos\theta & \sin\theta \\ -\sin\theta & \cos\theta \end{bmatrix}\begin{bmatrix} i_\alpha \\ i_\beta \end{bmatrix} \quad (46)$$

where θ=ωt represents the instantaneous grid voltage angle estimated by the PLL.

In the synchronous reference frame, the fundamental active and reactive current components appear as DC quantities, whereas the harmonic components appear as AC ripples. Therefore, a Low-Pass Filter (LPF) is employed to extract the fundamental current components,

$$i_{d,f} = LPF(i_d) \quad (47)$$

$$i_{d,f} = LPF(i_q) \quad (48)$$

The DC-link voltage is maintained at its reference value through a PI regulator. The voltage error is expressed as

$$e_v = V_{dc}^* - V_{dc} \quad (49)$$

The PI controller generates the reference active current,

$$i_{dc} = K_p e_v + k_i \int e_v dt \quad (50)$$

where Kp and Ki denote the proportional and integral gains, respectively.

The reference current components are obtained as

$$i_d^* = i_{d,f} + i_{dc} \quad (51)$$

$$i_q^* = 0 \quad (52)$$

where iq*=0 ensures unity power factor operation by eliminating reactive power exchange with the utility grid.

The reference currents are transformed back into the three-phase stationary frame through the inverse Park transformation,

$$\begin{bmatrix} i_\alpha^* \\ i_\beta^* \end{bmatrix} = \begin{bmatrix} \cos\theta & -\sin\theta \\ \sin\theta & \cos\theta \end{bmatrix}\begin{bmatrix} i_d^* \\ i_q^* \end{bmatrix} \quad (53)$$

followed by the inverse Clarke transformation,

$$\begin{bmatrix} i_a^* \\ i_b^* \\ i_c^* \end{bmatrix} = \begin{bmatrix} 1 & 0 \\ -\frac{1}{2} & \frac{\sqrt{3}}{2} \\ -\frac{1}{2} & -\frac{\sqrt{3}}{2} \end{bmatrix} \begin{bmatrix} i_\alpha^* \\ i_\beta^* \end{bmatrix} \quad (54)$$

The generated reference currents are compared with the actual converter currents in the hysteresis current controller. The current tracking error is defined as

$$e_i = i_{gabc}^* - i_{gabc} \quad (55)$$

The hysteresis controller maintains the tracking error within the hysteresis band,

$$-h \le e_i \le h \quad (56)$$

where h is the hysteresis bandwidth. The switching states of the converter are determined according to

$$\begin{cases} S = 1, & e_i < -h \\ S = 0, & e_i > h \end{cases} \quad (57)$$

The generated gate pulses are applied to the six switches of the bidirectional VSC, enabling the converter current to accurately track the reference current. Consequently, the converter injects compensating currents into the grid, suppresses harmonic components generated by nonlinear loads and power electronic converters, provides reactive power compensation, regulates the DC-link voltage, and maintains near-unity power factor. The proposed SRF-HCC control strategy therefore significantly improves the power quality, dynamic response, and stability of the grid-connected hybrid renewable energy-based EV charging station under both steady-state and transient operating conditions.

IX. SIMULATION RESULTS AND DISCUSSION

A. Performance Analysis of the Grid-Connected Bidirectional AC–DC Converter

The proposed grid-connected bidirectional AC–DC Voltage Source Converter (VSC) operating as a Shunt Active Power Filter (SAPF) is validated in MATLAB/Simulink under dynamic operating conditions. The simulation evaluates the converter in terms of grid voltage, grid current, load voltage, load current, and DC-link voltage regulation. Fig. 12 (a) shows the three-phase grid voltage. The converter maintains balanced sinusoidal voltages with a peak value of approximately ±180 V (about 127 V RMS per phase) at a frequency of 50 Hz throughout the 1 s simulation period. The absence of voltage distortion confirms stable grid operation. Fig. 12 (b) presents the three-phase grid current. During converter energization (0–0.1 s), the current reaches a peak value of approximately ±140 A. As the controller stabilizes the system, the current decreases and settles within ±20 A after 0.6 s, while remaining balanced and nearly sinusoidal. This demonstrates effective harmonic current compensation and controlled bidirectional power transfer. The three-phase load voltage shown in Fig. 12(c) remains balanced with a peak magnitude of approximately ±180 V during the entire simulation. The constant voltage amplitude indicates effective voltage regulation despite variations in renewable generation and EV charging demand. Fig. 12(d) illustrates the three-phase load current supplied to the nonlinear load. The current remains balanced with a peak value of approximately ±36 A throughout the simulation. Although the nonlinear load generates harmonic currents, these components are compensated by the VSC operating as a SAPF, preventing harmonic propagation into the utility grid. The DC-link voltage response is presented in Fig. 12 (e). At start-up, the DC-link voltage rises rapidly from 550 V to a maximum value of approximately 665 V, corresponding to an overshoot of about 10.8%. The controller quickly regulates the voltage to the reference value of 600 V within approximately 0.08 s. During load and renewable power variations, the DC-link voltage fluctuates only between 585 V and 630 V, demonstrating effective voltage regulation and fast dynamic response. Overall, the simulation results confirm that the proposed bidirectional AC–DC converter successfully regulates the 600 V DC-link, maintains balanced 180 V three-phase grid voltages, limits the steady-state grid current to approximately 20 A, supplies a balanced 36 A load current, and effectively compensates harmonic currents. Consequently, the converter operates efficiently as a Shunt Active Power Filter (SAPF), providing bidirectional power transfer, improved power quality, stable DC-link voltage, and reliable grid integration for the hybrid renewable energy-based EV charging station.

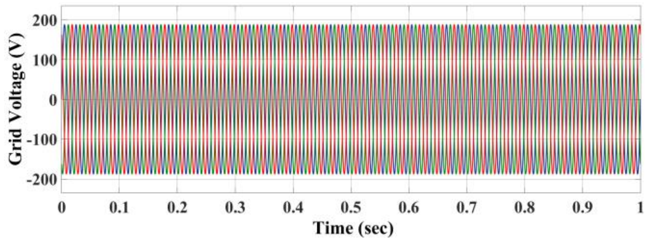

(a)

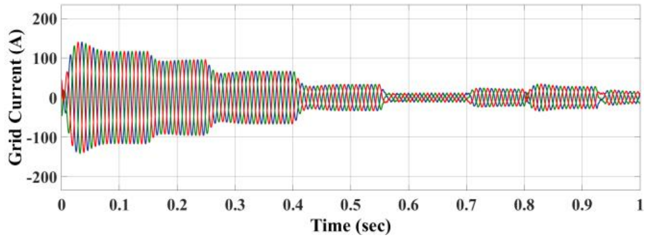

(b)

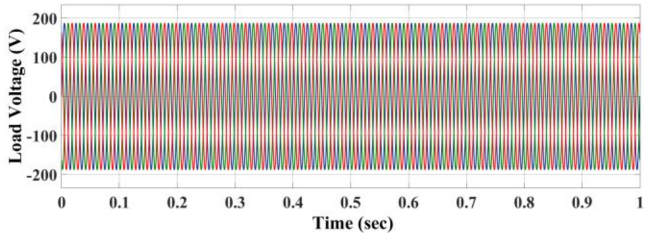

(c)

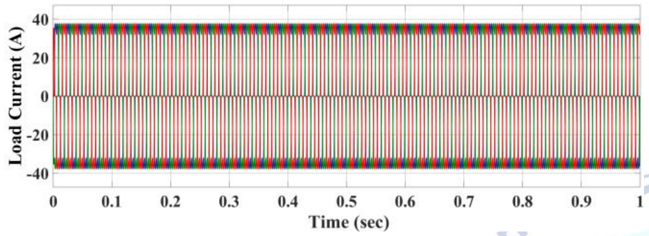

(d)

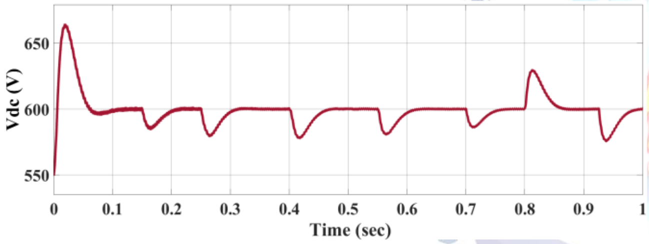

(e)

Fig. 12. Performance of the grid-connected bidirectional AC–DC voltage source converter operating as a shunt active power filter (SAPF): (a) three-phase grid voltage, (b) three-phase grid current, (c) three-phase load voltage, (d) three-phase load current, and (e) DC-link voltage response.

B. Performance Analysis of the Solar PV and Wind Energy Conversion System

The dynamic performance of the proposed solar PV and PMSG-based wind energy conversion system is evaluated under varying operating conditions. The simulation results demonstrate the effectiveness of the MPPT-controlled DC–DC boost converters in maintaining stable renewable energy extraction and supplying power to the common DC-link. Fig. 13 (a) shows the output voltage of the solar PV array. The PV voltage rapidly increases from 0 V to approximately 310 V at start-up and remains nearly constant throughout the simulation. Minor voltage variations are observed around 0.15 s and 0.25 s, after which the voltage quickly returns to its steady-state value, confirming effective voltage regulation by the boost converter and P&O MPPT controller. Fig. 13 (b) illustrates the output current of the solar PV array. Initially, the PV current reaches approximately 68 A. As the irradiance changes, the current decreases from 68 A to 48 A at 0.15 s, and subsequently to approximately 20 A at 0.25 s, where it remains constant for the remainder of the simulation. These variations indicate the MPPT controller continuously adjusts the operating point to extract the maximum available solar power under changing environmental conditions. Fig. 13 (c) presents the output current of the PMSG-based wind energy conversion system. During the initial interval, the wind generator produces a peak current of approximately ±70 A. As the wind speed decreases, the current magnitude reduces to about ±40 A at 0.40 s and further decreases to approximately ±18 A after 0.55 s. Despite these changes, the generated current remains balanced and sinusoidal, demonstrating stable operation of the PMSG, AC–DC rectifier, and DC–DC boost converter under varying wind conditions. Overall, the simulation results verify that the proposed renewable energy conversion system effectively extracts maximum power from both the solar PV array and the wind energy conversion system. The MPPT-controlled boost converters maintain stable output voltage, continuously track the maximum power operating point, and provide reliable power to the common DC-link for the hybrid renewable energy-based EV charging station.

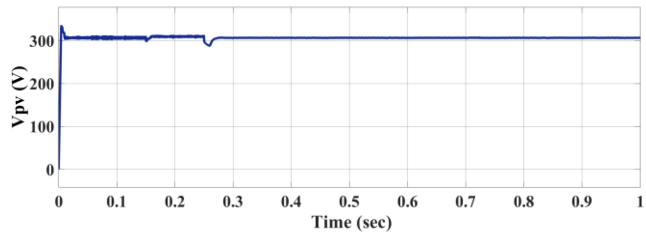

(a)

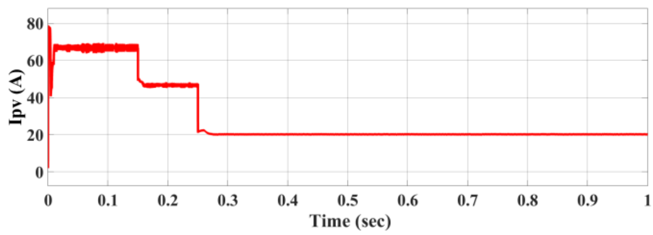

(b)

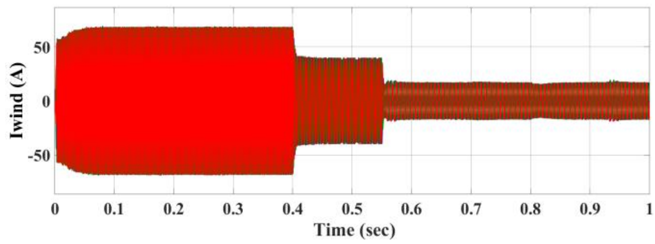

(c)

Fig. 13. Dynamic performance of the renewable energy sources: (a) solar PV output voltage, (b) solar PV output current, and (c) PMSG-based wind generator output current.

C. Performance Analysis of the EV Charging System

The dynamic performance of the proposed EV charging system is evaluated in terms of the EV battery voltage, charging/discharging current, and battery State of Charge (SOC). The simulation results verify the effectiveness of the bidirectional DC–DC converter in maintaining stable battery operation under different charging conditions. Fig. 14 (a) shows the EV battery voltage. At the beginning of the simulation, the battery voltage rapidly reaches approximately 220 V and remains nearly constant throughout the simulation period. A slight voltage increase to about 223 V is observed around 0.75 s, followed by stabilization at approximately 221 V, indicating effective voltage regulation by the bidirectional converter. Fig. 14 (b) illustrates the EV battery current. During the initial interval, the battery current is close to 0 A, indicating a steady operating condition. At approximately 0.70 s, the current decreases to about −25 A, representing the battery discharging mode (Vehicle-to-Grid, V2G). Subsequently, at 0.80 s, the current reverses to approximately +30 A, indicating Grid-to-Vehicle (G2V) charging operation. After 0.93 s, the charging current decreases and stabilizes around −15 A, demonstrating smooth transitions between charging and discharging modes. Fig. 14 (c) presents the EV battery State of Charge (SOC). The SOC remains nearly constant at approximately 79.32% during the simulation, with only a small variation between 79.319% and 79.3215% during the charging and discharging transitions. This confirms that the bidirectional converter effectively manages battery energy while maintaining stable battery operating conditions. Overall, the simulation results demonstrate that the proposed EV charging system provides stable battery voltage regulation, controlled bidirectional current flow, and reliable battery energy management. The coordinated operation of the bidirectional DC–DC converter enables seamless transitions between charging and discharging modes while maintaining the battery voltage and SOC within safe operating limits.

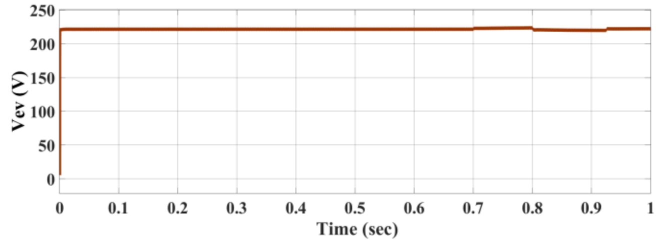

(a)

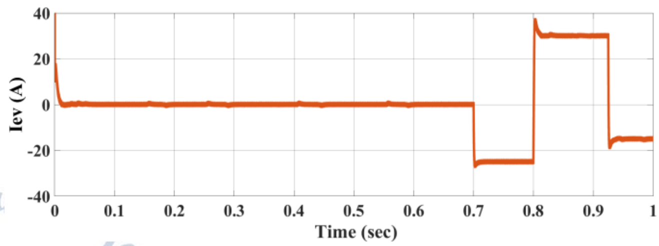

(b)

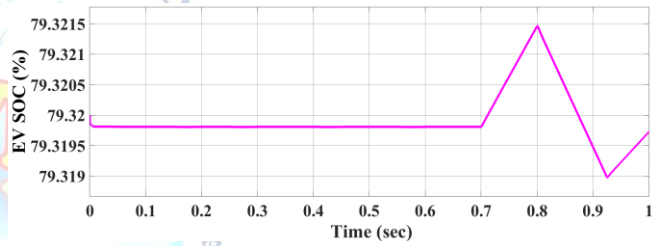

(c)

Fig. 14. Dynamic performance of the EV charging system: (a) EV battery voltage, (b) EV battery current, and (c) EV battery state of charge (SOC).

E. Power Flow Analysis of the Hybrid Renewable Energy-Based EV Charging Station

Fig. 15 presents the power flow characteristics of the proposed hybrid renewable energy-based EV charging station under varying operating conditions. The proposed energy management strategy coordinates power sharing among the solar PV array, PMSG-based wind energy conversion system, utility grid, EV charging station, and load. Initially, the solar PV and wind energy systems generate approximately 20 kW and 28 kW, respectively, while the load demand remains around 10 kW. As solar irradiance and wind speed decrease, the PV power reduces to approximately 8 kW, whereas the wind power decreases to about 6 kW. Despite these variations, the load demand is continuously satisfied through coordinated power management. The EV charging power remains close to 0 kW during the initial period. At approximately 0.70 s, the EV operates in V2G mode, delivering nearly 6 kW to the system. Subsequently, at 0.80 s, it switches to G2V mode, drawing approximately 7 kW for battery charging before returning to normal operation. The grid power initially reaches approximately −40 kW, indicating surplus renewable energy export to the utility grid. As renewable generation decreases and EV charging demand increases, the grid gradually supplies the required power to maintain continuous operation. These results demonstrate effective power coordination, improved renewable energy utilization, stable load supply, and reliable bidirectional EV charging.

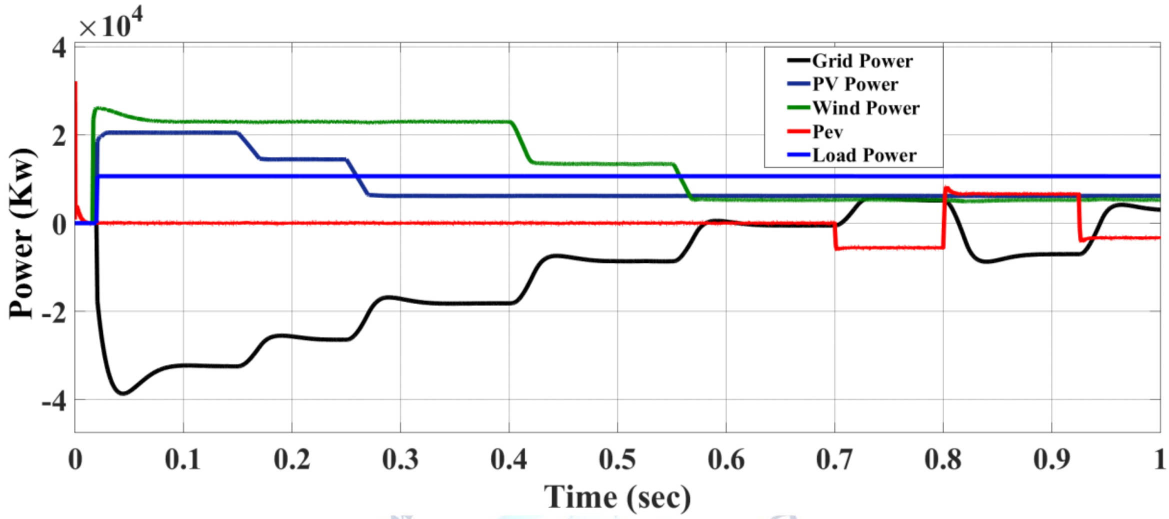

Fig. 15. Dynamic power flow of the proposed hybrid renewable energy-based EV charging station

X. CONCLUSION

This paper presented the design and control of a hybrid solar PV and PMSG-based wind energy EV charging station integrated with a battery energy storage system and a grid-connected bidirectional AC–DC voltage source converter. The proposed system effectively coordinated power exchange among the renewable energy sources, battery, utility grid, and EV charging station to ensure reliable and efficient operation under varying operating conditions. The P&O-based MPPT algorithm enabled maximum power extraction from the solar PV and wind energy systems, while the bidirectional DC–DC converter provided efficient charging and discharging of the EV battery. In addition, the SRF-based control strategy with a hysteresis current controller enabled the grid-connected converter to operate as a Shunt Active Power Filter (SAPF), improving power quality through harmonic current compensation, reactive power support, and stable DC-link voltage regulation. The simulation results confirmed that the proposed system achieved effective energy management, reliable bidirectional EV charging, improved renewable energy utilization, and stable power flow between the renewable sources, utility grid, and connected load. Therefore, the proposed EV charging system provides an efficient, reliable, and sustainable solution for future smart grid-integrated electric vehicle charging applications.

Conflict of interest statement

Authors declare that they do not have any conflict of interest.

REFERENCES

[1] G. Boyle, "Renewable electricity and the grid", 1st Ed., London, U.K., Earthscan, 2007.
[2] A. Y. Saber and G. K. Venayagamoorthy, "Plug-in vehicles and renewable energy sources for cost and emission reductions," IEEE Trans. Indust. Elect., vol. 58, no. 4, pp. 1229-1238, April 2011.
[3] S. Alepuz, S. Busquets-Monge, J. Bordonau, J. Gago, D. Gonzalez and J. Balcells, "Interfacing renewable energy sources to the utility grid using a three-level inverter," IEEE Trans. Indust. Elect., vol. 53, no. 5, pp. 1504-1511, Oct. 2006.
[4] R. Cárdenas, M. A. Pérez and J. C. Clare, "Guest editorial control and grid integration of MW-range wind and solar energy conversion systems," IEEE Trans. Indust. Elect., vol. 64, no. 11, pp. 8786-8789, Nov. 2017.
[5] Q. Zhong, "Power-electronics-enabled autonomous power systems: architecture and technical routes," IEEE Trans. Indust. Elect., vol. 64, no. 7, pp. 5907-5918, July 2017.
[6] J. M. Carrasco, L.G. Franquelo, J.T. Bialasiewicz, E. Galvan, R.C. PortilloGuisado, M.A.M. Prats, J.I. Leon, and N. Moreno-Alfonso,

"Power-electronic systems for the grid integration of renewable energy Sources: A survey," IEEE Trans. Indust. Elect., vol. 53, no. 4, pp. 1002- 1016, June 2006.
[7] P. K. Ray, S. R. Mohanty and N. Kishor, "Classification of power quality disturbances due to environmental characteristics in distributed generation system," IEEE Trans. Sustain. Energy, vol. 4, no. 2, pp. 302- 313, April 2013.
[8] M. Singh, V. Khadkikar, A. Chandra and R. K. Varma, "Grid interconnection of renewable energy sources at the distribution level with power-quality improvement features," IEEE Trans. Pow. Deliv., vol. 26, no. 1, pp. 307-315, Jan. 2011.
[9] F. Blaabjerg, R. Teodorescu, M. Liserre and A. V. Timbus, "Overview of control and grid synchronization for distributed power generation systems," IEEE Trans. Indust. Elect., vol. 53, no. 5, pp. 1398-1409, Oct. 2006.
[10] E. Afshari, G. R. Moradi, R. Rahimi, B. Farhangi, Y. Yang, F. Blaabjerg and S. Farhangi, "Control strategy for three-phase grid-connected pv inverters enabling current limitation under unbalanced faults," IEEE Trans. Indust. Elect., vol. 64, no. 11, pp. 8908-8918, Nov. 2017.
[11] L. E. Jones "Renewable energy integration: practical management of variability, uncertainty, and flexibility in power grids", 1st Ed., London, UK, Elsevier Inc., 2014.
[12] M. N. I. Sarkar, L. G. Meegahapola and M. Datta, "Reactive power management in renewable rich power grids: a review of grid-codes, renewable generators, support devices, control strategies and optimization algorithms," IEEE Access, vol. 6, pp. 41458-41489, 2018.
[13] D. Zhou, F. Blaabjerg, M. Lau and M. Tonnes, "Optimized reactive power flow of DFIG power converters for better reliability performance considering grid codes," IEEE Trans. Indust. Elect., vol. 62, no. 3, pp. 1552-1562, March 2015.
[14] K. Ma, M. Liserre, F. Blaabjerg and T. Kerekes, "Thermal Loading and lifetime estimation for power device considering mission profiles in wind power converter," IEEE Trans. Pow. Elect., vol. 30, no. 2, pp. 590- 602, Feb. 2015.
[15] A. Anurag, Y. Yang and F. Blaabjerg, "Thermal performance and reliability analysis of single-phase PV inverters with reactive power injection outside feed-in operating hours," IEEE Jour. Emerg. Sel. Top. Pow. Elect., vol. 3, no. 4, pp. 870-880, Dec. 2015.
[16] R. K. Varma, S. A. Rahman and T. Vanderheide, "New control of PV solar farm as STATCOM (PV-STATCOM) for increasing grid power transmission limits during night and day," IEEE Trans. Pow. Deliv., vol. 30, no. 2, pp. 755-763, April 2015.
[17] S. Roy Ghatak, S. Sannigrahi and P. Acharjee, "Multi-objective approach for strategic incorporation of solar energy source, battery storage system, and DSTATCOM in a smart grid environment," IEEE Syst. Journal, Early Access, 2019.
[18] X. Guo, W. Wu and Z. Chen, "Multiple-complex coefficient-filter-based phase-locked loop and synchronization technique for three-phase gridinterfaced converters in distributed utility networks," IEEE Trans. Indust. Elect., vol. 58, no. 4, pp. 1194-1204, April 2011.
[19] X. He, H. Geng and G. Yang, "A Generalized Design Framework of Notch Filter Based Frequency-Locked Loop for Three-Phase Grid Voltage," IEEE Trans. Indust. Elect., vol. 65, no. 9, pp. 7072-7084, Sept. 2018.
[20] Hurng- Liahng Jou, Kuen- Der Wu, Jinn- Chang Wu and Wen-Jung Chiang, "A three-phase four- wire power filter comprising a three-phase three-wire active filter and a zig-zag transformer," IEEE Trans. Power Electron., vol. 23, no. 1, pp. 252- 259, January 2008.
[21] María Isabel Milanés, Enrique Romero Cadaval and Fermín Barrero González, "Comparison of Control Strategies for Shunt Active Power Filters in Three-Phase Four-Wire Systems," IEEE Transactions on Power Electronics, vol. 22, no. 1, pp.229-236, Jan. 2007.
[22] B Singh, K Al-Haddad and A Chandra, "Active power filter with sliding mode control," IEE Proc. on Generation, Transmission and Distribution, vol. 144, no.6 pp:564 – 568., Nov. 1997.
[23] B. Singh, K. Al. Haddad and A. Chandra, "A review of active filters for power quality improvement," IEEE Trans. Industrial Electronics, vol. 46, pp. 960-971, October 1999.
[24] C.A. Quinn, and N. Mohan, "Active filtering of harmonic currents in three-phase, four-wire systems with three-phase and single-phase nonlinear loads," in Proc. of APEC '92, Feb. 1992, pp. 829 – 836.
[25] Wenchao Song, and Alex Q. Huang, "Fault-Tolerant Design and Control Strategy for Cascaded H-Bridge Multilevel Converter-Based STATCOM," IEEE Transactions on Industrial Electronics, Vol. 57, No. 8, pp.2700-2708, August 2010.
[26] Vishal Verma, Bhim Singh, Ambrish Chandra, and Kamal Al-Haddad, "Power Conditioner for Variable-Frequency Drives in Offshore Oil Fields," IEEE Transactions on Industry Applications, Vol. 46, No. 2, pp. 721-738, March/April 2010.
[27] Xuancai Zhu, Xiao Li, Guoqiao Shen, and Dehong Xu, "Design of the Dynamic Power Compensation for PEMFC Distributed Power System," IEEE Transactions on In dustrial Electronics, Vol. 57, No. 6, pp. 1935- 1944, June 2010.
[28] S. Rahmani, N. Mendalek and K. Al-Haddad," Experimental Design of a Nonlinear Control Technique for Three-Phase Shunt Active Power Filter," accepted for IEEE Transactions on Industrial Electronics.